Referee #2

Comment B1

This manuscript presents a new implementation of a dynamic grassland density scheme within the ORCHIDEE land surface model. The proposed approach allows grass density to vary in response to physiological carbon reserves, enabling a more flexible and ecologically realistic representation of vegetation cover, particularly under semi-arid conditions. The overall scheme is well justified. The authors evaluate this scheme using multiple lines of evidence, including relationships between precipitation and grass density, frequency of grassland mortality events, and comparisons with satellite-derived LAI products. The proposed dynamic density scheme effectively mitigates key limitations of the original model in simulating grassland dynamics under semi-arid conditions, thereby offering substantial value for model development and holding considerable potential for broader scientific impact. The manuscript is well written. However, the current version of the manuscript requires some improvements in the rigor and comprehensiveness of the model evaluation.

Response

We thank the reviewer for the positive assessment of our work and for the constructive feedback regarding the need to enhance the rigor and comprehensiveness of the model evaluation. We appreciate the constructive criticism as it will strengthen this aspect of the manuscript. In the revised version, we have carefully addressed this point, as detailed in our point-by-point responses below.

Comment B2

(1) The evaluation relies primarily on indirect indicators (e.g., LAI, mortality frequency) without sufficient direct evidence that the model accurately reproduces observed spatial patterns of grass density or vegetation coverage. Comparison against datasets such as vegetation coverage (e.g., vegetation fractional coverage data) may provide insights in the model improvements?

Response

We thank the reviewer for this constructive suggestion. As recommended, we sought a direct comparison against a fractional vegetation cover dataset to test for the model's ability to represent spatial patterns.

Following this recommendation, we have performed a rigorous evaluation for the simulated fractional vegetation cover (FVC) against the Copernicus Land Monitoring Service FCOVER dataset (Copernicus Land Monitoring Service, 2020). We selected the year 2004 for this comparison, as it matches the static global land cover map used throughout this study. The FCOVER product (originally at ~0.003° resolution) was regridded to our model's $2^{\circ}\times2^{\circ}$ resolution. To ensure a fair comparison, we:

1. Calculated the corresponding fractional vegetation cover (*FVC*) specifically from the targeted grassland PFTs within ORCHIDEE using the equation:

$$FVC = D_{\text{temp C3}} \times V_{\text{fra,temp C3}} + D_{\text{C4}} \times V_{\text{fra,C4}} + D_{\text{trop C3}} \times V_{\text{fra,trop C3}}$$

where $D_{\text{temp C3}}$, D_{C4} , and $D_{\text{trop C3}}$ are the simulated grassland density (1.0 for the fixed density approach, 0.05–1.0 for our new dynamic density approach) and $V_{\text{fra,temp C3}}$, $V_{\text{fra,C4}}$, and $V_{\text{fra,trop C3}}$ are the fractional area of each grassland PFT (temperate C₃, C₄, tropical C₃) in one grid cell.

2. Applied a (semi-)arid region mask (based on Zomer et al., 2022) to focus the analysis on our target ecosystems where grasslands dominate and exclude the canopy cover from other vegetation as much as possible.

The results of this direct comparison (Fig. S7) illustrated the improvements brought by the new dynamic approach. Regarding the spatial patterns, the spatial correlation (Pearson's r) between the model and the FCOVER dataset increased from a r=0.11 with the old approach to r=0.24 with our new (dynamic) approach. The new approach also achieved a lower RMSE (0.22) compared to the old approach (0.26).

This improvement was obvious over the western United States, Asia, southern Africa, and Australia (Fig. S7), where the new dynamic scheme simulated a lower and more realistic *FVC*, in closer agreement with the dataset, compared to the fixed density approach.

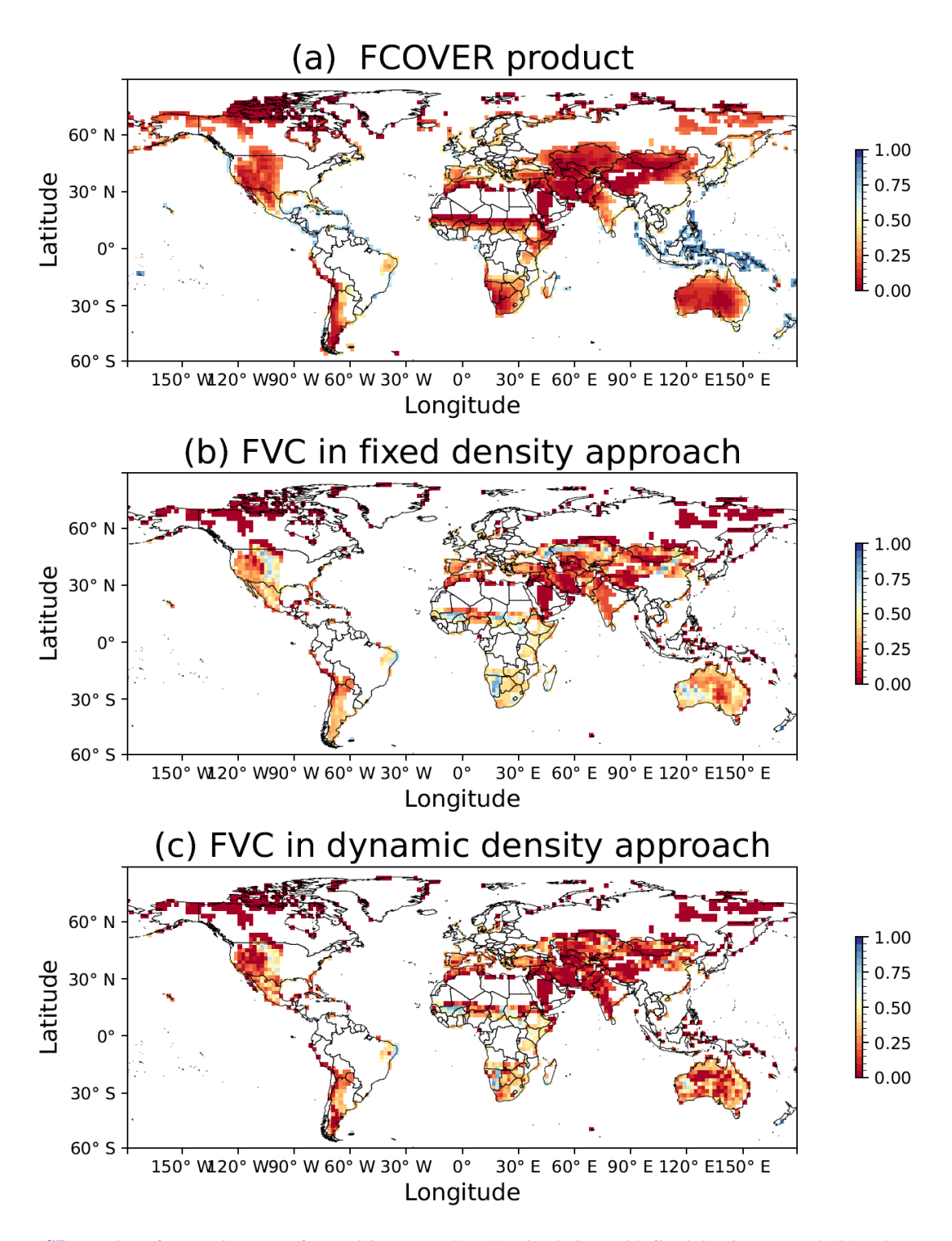


Figure S7. Fraction of vegetation cover from FCOVER product (a), simulations with fixed density approach (b) and dynamic density approach (c) in 2004.

It should be noted that two main caveats apply to this comparison, which can explain the remaining deviation from observations: (1) In (semi-)arid regions, the FCOVER product includes all green vegetation (e.g., shrubs, crops), whereas our calculation here includes only the grassland PFTs that we improved. (2) The current model version does not yet account for disturbances like grazing or fire (Chang et al., 2016; Chang et al., 2021), which are known to reduce *FVC* and are implicitly included in the satellite observations.

However, the fact that our new approach achieved a clear relative improvement: the spatial correlation (Pearson's r) with the FCOVER data increased from 0.11 (with the old approach) to 0.24 (with our new dynamic approach), alongside a 15% reduction in RMSE, despite these known model and data differences. It thus provides the evidence that our new dynamic density scheme is a substantial step toward greater ecological realism.

The corresponding revisions regarding the direct comparison of *FVC* were implemented in the Methods (lines 204–216):

"Furthermore, the simulated fractional vegetation cover was compared against the Copernicus Land Monitoring Service FCOVER product (Copernicus Land Monitoring Service, 2020). We selected the year 2004 for this comparison, as it matches the static global land cover map used throughout this study. The FCOVER product (originally at ~0.003° resolution) was regridded to our model's 2°×2° resolution using RemapCon (Jones, 1998; Goudiaby et al., 2024) in the Climate Data Operators library for Linux. To ensure a fair comparison, we calculated the corresponding fractional vegetation cover (*FVC*) specifically from the targeted grassland PFTs within ORCHIDEE using the equation:

$$FVC = D_{\text{temp C3}} \times V_{\text{fra,temp C3}} + D_{\text{C4}} \times V_{\text{fra,C4}} + D_{\text{trop C3}} \times V_{\text{fra,trop C3}}$$

$$\tag{6}$$

where $D_{\text{temp C3}}$, D_{C4} , and $D_{\text{trop C3}}$ are the simulated grassland density (1.0 for the fixed density approach, 0.05–1.0 for our new dynamic density approach) and $V_{\text{fra,temp C3}}$, $V_{\text{fra,C4}}$, and $V_{\text{fra,trop C3}}$ are the fractional area of each grassland PFT (temperate C₃, C₄, tropical C₃) within one grid cell.

Given that this study aims to improve grassland density simulation, the comparison of *FVC* focused specifically on grasslands. To isolate the target ecosystems where grasslands dominate and exclude the canopy cover from other vegetation as much as possible, we applied a (semi-)arid region mask based on the aridity index map by Zomer et al. (2022)."

Results (lines 376–383):

"The dynamic density approach was further evaluated against a comparison of FVC with a global satellite-based FCOVER product (Copernicus Land Monitoring Service, 2020) (Fig. S7). The spatial correlation (Pearson's r) between the model and the FCOVER data increased from r = 0.11 with the fixed density approach to r = 0.24 with the dynamic density approach. The dynamic density approach also exhibited a lower RMSE (0.22) compared to the fixed density approach (0.26). This improvement was particularly evident in western United States, Asia, southern Africa, and Australia, where the dynamic scheme simulated a lower and more realistic FVC (Fig. S7c), in better agreement with the FCOVER dataset, compared to the fixed density approach (Fig. S7b). Such regional-scale improvement is consistent with the findings from the regional field-based comparisons."

Discussion (lines 530–537):

"As shown in the results (Sect. 3.2), the direct *FVC* comparison against the FCOVER satellite product (Copernicus Land Monitoring Service, 2020) also supported the new dynamic approach, which improved both spatial correlation (r) and RMSE. There are two main caveats in this comparison, which likely explain the deviation from observations: (1) In (semi-)arid regions, the FCOVER product includes all green vegetation (e.g., shrubs, crops), whereas our calculation was focused only on the grassland PFTs we improved. (2) The current model does not yet account for key disturbances like grazing or fire, which are known to affect *FVC* and

are implicitly included in the satellite observations (Chang et al., 2016; Chang et al., 2021). Nevertheless, the fact that our new scheme showed a clear improvement despite these known mismatches underscores the robustness of the new dynamic density approach."

In addition, to further enhance the rigor and comprehensiveness of our evaluation, we have also added five new regional case studies comparing the model against field-based observations, covering diverse ecosystems, including a temperate European grassland (France), the Eurasian steppes (Mongolia), a North American meadow (USA), a Sahelian rangeland (Senegal), and a semi-arid grass—shrub community (Australia).

Although the metrics from the field-based observation are not identical to the grassland density defined in our study, to mitigate this gap, we have selected the five case studies (Booth et al., 2005; Dusseux et al., 2014; John et al., 2018; Melville et al., 2019; Diatta et al., 2023) that provide metrics conceptually similar to our definition of density: the fractional area occupied by conceptual individuals.

The results from this comparison are summarized in Table 1. The simulated annual mean grass densities show an overall good agreement with field observations, supporting the ecological realism of the model. For example, in France, observed value for grassland density range from 0.91 to 0.99, while the model simulated 0.95; similar consistency was found in the United States (0.68 observed vs 0.63 simulated) and Australia (0.10–0.60 observed vs 0.15 and 0.50 simulated). In Senegal, the simulated value of 0.18 remains near the lower bound of the observed range (0.06 to 0.79). In Mongolia, the different steppe types (typical, meadow, and desert) represent plot-based locations. This presents a scale mismatch when comparing them to the coarse spatial resolution in ORCHIDEE, but the results are still in agreement.

Details of this new evaluation and its rationale have been added (lines 183–197) to the new section "2.3 Model evaluation against regional field observations and global dataset" in Methods, as:

"In order to directly assess the ecological realism of the simulated grassland density, we compared model outputs with field-based estimates from five published regional case studies. These studies span a range of grassland ecosystems: a temperate European grassland in France (Dusseux et al., 2014), the Eurasian steppe on the Mongolian Plateau (John et al., 2018), a meadow in the USA (Booth et al., 2005), a Sahelian rangeland in Senegal (Diatta et al., 2023), and a grass-shrub community in Australia (Melville et al., 2019), as listed in Table 1.

We acknowledge that the metrics from field-based observation are not identical to the grassland density defined in our study. However, the five case studies provide metrics that are thought to be sufficiently similar to be compared to the metric in ORCHIDEE, i.e., the fractional area occupied by conceptual individuals (Fig. 1a–b). The case-studies provide the area-based geometric estimates—either by counting points classified as vegetation within quadrats (John et al., 2018; Diatta et al., 2023), along transects (Booth et al., 2005; Melville et al., 2019), or from downward-facing hemispherical photographs to estimate green vegetation cover (Dusseux et al., 2014). Detailed descriptions of each dataset, including observed and corresponding simulated values, measurement methods, and caveats of the selected methods, are provided in Table 1. The hemispherical photography method may be

influenced by plant height and leaf area (Dusseux et al., 2014); the effects of grazing were controlled by selecting fenced sites (Diatta et al., 2023); and the observational sites included not only grasses but also forbs and shrubs, although grasses were dominant (Melville et al., 2019)."

The full results interpretation has been added to the Results subsection in section "3.2 Evaluation of simulated grassland density" (lines 366–375), as:

"The simulated grassland density was compared against direct field-based estimates for five regional case studies (Table 1). Over temperate grassland in France, the simulated density of 0.95 was within the observed range of 0.91 to 0.99 (Dusseux et al., 2014). This consistency extended to the Upper Beaver Meadows site in North America, with a simulated density of 0.63 that approached the observed mean of 0.68 (Booth et al., 2005). For the desert steppe (with the cold desert climate) of the Mongolian Plateau, the simulated value of 0.27 was just outside the observed range of 0.10–0.26 (John et al., 2018). Furthermore, simulated average densities for typical steppes characterized by the semi-arid climate (0.40) and meadow steppes characterized by the subarctic climate (0.63) fell within their respective observed ranges of 0.34–0.50 and 0.45–0.78 (John et al., 2018). In the Sahelian fenced rangeland of Senegal, the simulated density of 0.18 was in the low range of the large observed range of 0.06 to 0.79. Finally, for the mixed grass-shrub community in Australia, both the simulated C4 (0.15) and tropical C3 (0.50) grass densities were consistent with the field-based range of 0.1 to 0.6 (Melville et al., 2019)."

The discussion of strengths and limitations was included in the section "4.1 The implementation of dynamic grassland density" (lines 515–529), as:

"The evaluation against five case studies (Table 1) gives confidence in the model's ability to represent grassland density across different grass PFTs and locations. The close agreement at all the five sites suggests our model accurately captures the central tendency of grassland density. Despite these encouraging results, this evaluation should be interpreted with caution due to several key uncertainties. The primary challenge is the conceptual mismatch between our simulated "density" and the observational metrics. The mismatch was mitigated by selecting the closest available conceptual analogues (Sect. 2.3). However, the discrepancies cannot be fully eliminated. For example, in the Australian grass-shrub community (Melville et al., 2019), the field-based metric unavoidably includes shrubs, thus resulting in higher values compared to a pure grassland ecosystem. While the close agreement (Table 1) suggests the dynamic density approach captured the dominant grass trend, the shrublands in Australia might also be misclassified as grasslands in the PFT maps in ORCHIDEE, which would lead to our model simulating grasslands in the shrub-contaminated areas. This alignment may therefore stem partly from this PFT misclassification. In addition, the scale mismatch between plot-level field data and the model's coarse grid-cell resolution is another source of uncertainty, particularly in heterogeneous landscapes like the Mongolian Plateau. Despite this spatial discrepancy, the result that our simulated value range aligned with the observed range suggests the new approach captures the ecological gradient across different steppes: with higher values in meadow steppe, medium values in typical steppe, and lower values in desert steppe (Booth et al., 2005; Dusseux et al., 2014; John et al., 2018; Melville et al., 2019; Diatta et al., 2023)."

Below is the new Table 1 added in the manuscript:

Table 1. Evaluation of simulated grassland density from ORCHIDEE against field-based estimates from various grassland sites (all values in m² m⁻²).

| Site/Region | Observed Value | Simulated Value | Observational Method and Caveats | Model Value Extraction |
|---|------------------|--|--|---|
| Yar Watershed, France | 0.91–0.99 | 0.95 | Fraction of vegetation cover from downward-facing hemispherical photographs taken approximately 1 m above the canopy (Dusseux et al., 2014). Caveat: The observed value is affected by plant height and leaf area, which might influence the consistency with grassland density. | Temperate C ₃ grassland density extracted at 3° W, 47° N. |
| Mongolian Plateau (meadow steppe) | 0.45–0.78 | 0.63±0.35 | Canopy cover from grid-square counting, measured by counting the number of 10×10 grid mesh filled with vegetation within a 0.5×0.5m quadrat | Temperate C ₃ grassland density extracted for each steppe type. See Note* for coordinates. |
| Mongolian Plateau (typical steppe) | 0.34–0.5 | 0.40±0.24 | (John et al., 2018). | |
| Mongolian Plateau (desert steppe) | 0.1–0.26 | 0.27±0.06 | | |
| The Upper Beaver Meadows, USA | 0.68 (0.52–0.86) | 0.63 | Green cover from point-intercept transects, classifying a functional group (green vegetation or bare ground) at points spaced every 30 cm along two parallel 50-meter transects (for a total of 166 points per transect) by a two-member crew (Booth et al., 2005). | Temperate C ₃ grassland density extracted at 105° W, 39° N. |
| Ferlo, Senegal | 0.06–0.79 | 0.18 | Visual estimation of vegetation coverage in 1 m ² quadrats. Selected the ungrazed, fenced site (Diatta et al., 2023). Caveat: Data is from a fenced, ungrazed site to exclude grazing effects. | The C ₄ grassland density extracted at 15° W, 15° N. |
| Fowlers Gap, Australia | 0.1-0.6 | 0.15 (C ₄); 0.50 (tropical C ₃) | Photosynthetic vegetation fraction from star transects, by recording every meter along three 100-meter tapes laid out in a star pattern (Melville et al., 2019). Caveat: The field site is a mixed community of grasses, forbs and shrubs, not pure grassland. | The C ₄ and tropical C ₃ grassland densities extracted at 141° E, 31° S. |

*Note: According to Figure 1 in John et al. (2018), we delineated three types of steppe on the Mongolian Plateau in ORCHIDEE: 97° E–103° E, 45° N–47° N in the meadow steppe, excluding other steppe types within this rectangle; 111° E–117° E, 39°N–47°N in the typical steppe, excluding forest meadow and meadow steppe within this range; 89°E–111°E, 39°N–45°N in the desert steppe, excluding desert and typical steppe areas.

References:

Booth, D. T., Cox, S. E., Fifield, C., et al.: Image analysis compared with other methods for measuring ground cover, Arid Land Res. Manag., 19, 91–100, https://doi.org/10.1080/15324980590916486, 2005.

Chang, J., Ciais, P., Gasser, T., et al.: Climate warming from managed grasslands cancels the cooling effect of carbon sinks in sparsely grazed and natural grasslands, Nat. Commun., 12, 118, https://doi.org/10.1038/s41467-020-20406-7, 2021.

Chang, J., Ciais, P., Herrero, M., et al.: Combining livestock production information in a process-based vegetation model to reconstruct the history of grassland management, Biogeosciences, 13, 3757–3776, https://doi.org/10.5194/bg-13-3757-2016, 2016.

Copernicus Land Monitoring Service: Fraction of Green Vegetation Cover 2014-present (raster 300 m), global, 10-daily—version 1. Copernicus Land Monitoring Service [Data set]. https://doi.org/10.2909/09578c73-4f5d-4d2c-90ff-4e17fb7dbf69, 2020 (last access: 01/11/2025).

Diatta, O., Ngom, D., Ndiaye, O., Diatta, S., and Taugourdeau, S.: Structure and phenology of herbaceous stratum in the Sahelian rangelands of Senegal, Grasses, 2, 98–111, https://doi.org/10.3390/grasses2020009, 2023.

Dusseux, P., Vertès, F., Corpetti, T., et al.: Agricultural practices in grasslands detected by spatial remote sensing, Environ. Monit. Assess., 186, 8249–8265, https://doi.org/10.1007/s10661-014-4001-5, 2014.

John, R., Chen, J., Giannico, V., et al.: Grassland canopy cover and aboveground biomass in Mongolia and Inner Mongolia: Spatiotemporal estimates and controlling factors, Remote Sens. Environ., 213, 34-48, https://dx.doi.org/10.1016/j.rse.2018.05.002, 2018.

Melville, B., Fisher, A., and Lucieer, A.: Ultra-high spatial resolution fractional vegetation cover from unmanned aerial multispectral imagery, Int. J. Appl. Earth Obs. Geoinf., 78, 14–24, https://doi.org/10.1016/j.jag.2019.01.013, 2019.

Zomer, R. J., Xu, J., and Trabucco, A.: Version 3 of the Global Aridity Index and Potential Evapotranspiration Database, Sci. Data, 9, 409, https://doi.org/10.1038/s41597-022-01493-1, 2022.

Comment B3

(2) The simulated LAI was compared with MODIS and Sentinel-2 LAI. However, it does not convincingly show how the dynamic density scheme improves the LAI simulation. The differences in LAI between the dynamic and fixed approaches are illustrated (e.g., Fig. 8), while there is little quantitative assessment of the improvement. The figures do not clearly highlight regions where the new scheme reduces model—data mismatches. Without clearer metrics or spatial diagnostics, the added value of the new scheme remains ambiguous. Furthermore, it is not clear whether the seasonality of LAI is improved due to the new scheme.

Response

We thank the reviewer for this critical and constructive feedback. We agree that a comprehensive and clear quantitative assessment of LAI is essential to demonstrate the added value of the new scheme. We have conducted a new, three-part quantitative analysis specifically designed to evaluate the improvements in LAI simulation against MODIS dataset. To more accurately assess the model's improvement in critical areas, all subsequent analyses applied a mask for (semi-)arid regions based on the aridity index map (Zomer et al., 2022). This allows us to focus on the scheme's performance in these key water-stressed environments.

First, we conducted a global-scale comparison of the mean annual grassland LAI simulated from both the old (fixed density) and new (dynamic density) approaches against the MODIS dataset. The statistics confirm a consistent, albeit modest, improvement with the new scheme: the Pearson's correlation (r) increased from 0.51 to 0.56, and the RMSE decreased from 0.60 to 0.59. This demonstrates a statistically better performance for the new approach at the global scale.

Regarding spatial diagnostics, we focused on the four representative semi-arid regions: Australia, southern Africa, Central Asia, and South America (Fig. S11a). These sites were chosen as they represent the large contiguous grassland ecosystems within the semi-arid domain on their respective continents. We found that the new dynamic scheme shows clear and consistent advantages in capturing the spatial patterns of LAI. Compared to the MODIS dataset, the coefficient of determination (R²) increased or remained unchanged in all four regions with the new approach (Fig. S11b–e, Table 2). The RMSE decreased in three of the four regions (Australia, Central Asia, and southern Africa).

Finally, we assessed the model's ability to simulate the mean seasonal cycle. The improvement is most dramatic in southern Africa (Fig. S12b). The old approach failed to capture the dry-season LAI minimum (August–October), whereas the new approach mitigates this major bias. The new dynamic density approach increased the seasonal correlation (r) with MODIS from 0.77 to 0.93, compared to the fixed density approach. However, seasonality in Australia (Fig. S12a) and South America (Fig. S12d) did not show improvements (Table 2). This suggests that other factors (e.g., processes not yet included or parameters needing optimization) may be dominant drivers of LAI seasonality in those specific regions, which helps identify clear pathways for future model development.

In summary, this quantitative assessment confirms the value of the dynamic scheme while also illuminating its limitations. The scheme's strengths are the clear, measurable improvements in global and regional spatial patterns of LAI (Fig. S11, Table 2), and the pronounced improvement in seasonal dynamics in key regions like Southern Africa (Fig. S12). Its limitations are that the global-scale improvements were modest, and the seasonal improvements were not equally significant in all regions (e.g., Australia, South America). It thus serves a crucial diagnostic purpose: it validates the new approach's effectiveness while simultaneously helping us target other key phenological processes and specific regions for further improvement. These new analyses have been added to the revised manuscript in the Results (lines 473–484):

"To refine the LAI analysis, a mask was applied to (semi-)arid regions identified by Zomer et al. (2022), focusing on water-stressed environments. Globally, compared with the MODIS dataset (Fig. 8a), the Pearson correlation coefficient (r) increased from 0.51 to 0.56, and the RMSE decreased from 0.60 to 0.59 when transitioning from the fixed density to the dynamic density approach. Spatially, statistical analysis was conducted for the four representative semi-arid regions: Australia, southern Africa, Central Asia, and South America (Fig. S11a), which were chosen as they represent the large contiguous grassland ecosystems within the semi-arid domain on their respective continents. In all four regions, the coefficient of determination (R²) improved or remained unchanged under the dynamic density approach (Fig. S11b-e, Table 2), while RMSE decreased in three regions (Australia, Central Asia, and southern Africa). Moreover, the dynamic density approach enhanced the seasonal dynamics in southern Africa (Fig. S12b, Table 2), successfully capturing the dry-season LAI minimum (August-October) that the fixed density approach failed to reproduce. The new dynamic density approach increased the seasonal correlation (r) with MODIS from 0.77 to 0.93, compared to the fixed density approach. In contrast, seasonality in Australia (Fig. S12a) and South America (Fig. S12d) did not show improvements (Table 2)."

Discussion (lines 652–657):

"The global and regional quantitative assessment against the MODIS dataset demonstrates that the dynamic density approach yields consistent, albeit modest improvements in grassland LAI (Figs. S11, S12). However, this analysis also reveals that the overall global improvement is minor, and that the issue of LAI seasonality persists. It is important to note that LAI seasonality is driven by the phenology subroutine in ORCHIDEE, which was not modified by our new dynamic density approach. Improving this phenology remains a separate, long-standing challenge in Earth System Models. This underlying issue is relevant, though, as these persistent phenological issues likely contribute to the remaining mortality events in our simulations."

The newly added Table 2, Figure S11 and Figure S12 are shown below.

Table 2. Statistical comparison of simulated grassland LAI (from this study) against MODIS LAI across four regions: Australia, southern Africa, Central Asia, and South America. Statistics include the coefficient of determination (R^2) and RMSE for mean annual LAI, and Pearson's r and RMSE for LAI seasonality.

| _ | · | Mean annual grasslands | LAI | |
|--------------------|------------------------|--------------------------|------------------------|--------------------------|
| Regions | | \mathbb{R}^2 | RMSE | |
| | Fixed density approach | Dynamic density approach | Fixed density approach | Dynamic density approach |
| Australia | 0.58 | 0.72 | 0.39 | 0.36 |
| Southern Africa | 0.13 | 0.21 | 0.58 | 0.55 |
| Central Asia | 0.38 | 0.40 | 0.28 | 0.27 |
| South America | 0.45 | 0.45 | 0.79 | 0.81 |
| | | LAI seasonality | | |
| Regions | | r | RMSE | |
| | Fixed density approach | Dynamic density approach | Fixed density approach | Dynamic density approach |
| Australia | -0.60 | -0.67 | 0.47 | 0.54 |
| Southern Africa | 0.77 | 0.93 | 0.14 | 0.14 |
| Central Asia | 0.30 | 0.31 | 0.62 | 0.62 |
| South America | 0.62 | 0.60 | 0.63 | 0.67 |

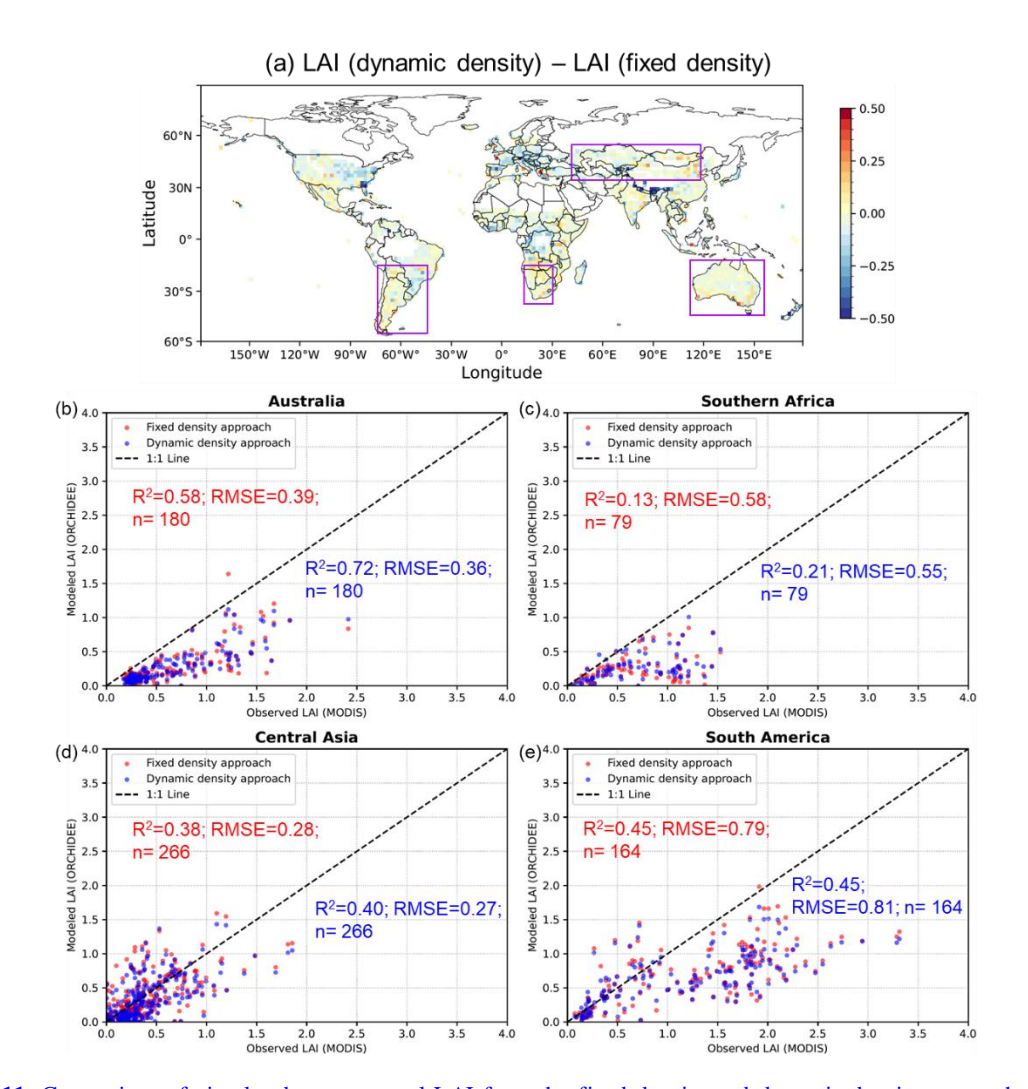


Figure S11. Comparison of simulated mean annual LAI from the fixed density and dynamic density approaches against MODIS LAI. (a) Global map of the mean annual LAI difference (Dynamic density approach – Fixed density approach). Purple boxes highlight the four representative regions: (b) Australia (113° E–155° E, 45° S–11° S), (c) southern Africa (13° E–35° E, 23° S–15° S), (d) Central Asia (41° E–119° E, 33° N–55° N), and (e) South America (75° W–45° W, 55° S–15° S). (b–e) Scatter plots comparing modelled LAI (ORCHIDEE) against observed LAI (MODIS) for each region. Red points and text correspond to the fixed density approach, while blue points and text correspond to the dynamic density approach. Statistical metrics (R², RMSE, and sample size n) are shown for each approach. The dashed black line is the 1:1 line. All values represent mean annual averages for the 2004–2020 period. The analysis for (b-e) was restricted to semi-arid and arid regions (based on the aridity index from Zomer et al., 2022) to ensure the comparison focused on grassland-dominated ecosystems. Both the "Observed LAI (MODIS)" (x-axis) and the "Modeled LAI (ORCHIDEE)" (y-axis) represent grassland LAI.

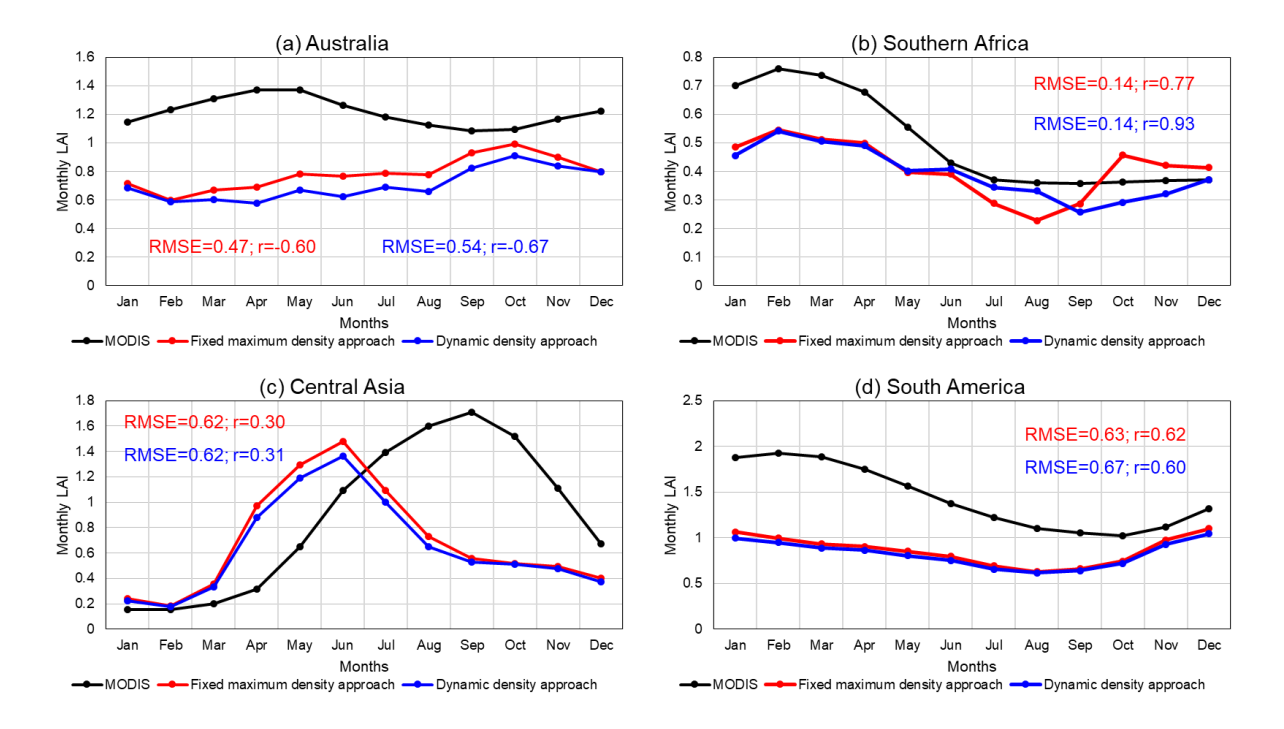


Figure S12. Average seasonal cycle of LAI, comparing MODIS observations with simulations from the fixed density (red line) and dynamic density (blue line) approaches. The comparison is shown for four representative regions: (a) Australia, (b) southern Africa, (c) Central Asia, and (d) South America. All data represent the mean monthly values, averaged over the 2004–2020 period. The analysis was restricted to semi-arid and arid regions (based on the aridity index from Zomer et al., 2022) to ensure the comparison focused on grassland-dominated ecosystems, where both MODIS and simulated LAI represent grassland LAI. Statistical metrics (Pearson's r and RMSE) for each approach against MODIS are shown in the corresponding colours.

References:

Zomer, R. J., Xu, J., and Trabucco, A.: Version 3 of the Global Aridity Index and Potential Evapotranspiration Database, Sci. Data, 9, 409, https://doi.org/10.1038/s41597-022-01493-1, 2022.

Comment B4

Minor remarks:

Figure 2 is unnecessary. The processes are quite simple and can be well understand with text only.

Response

Thank you for this comment. We agree that Figure 2 is unnecessary, accordingly, and we have removed this figure in the revised manuscript.